Supporting Information for

Adding a Second Quinol to a Redox-Responsive MRI Contrast Agent Improves its Relaxivity Response to H_2O_2

Meng Yu,[†] Meghan B. Ward,[†] Alicja Franke,[§] Stephen L. Ambrose,[†] Zachary L. Whaley,[†] Thomas Miller Bradford,[†] John D. Gorden,[†] Ronald J. Beyers,[‡] Russell C. Cattley,[¶] Ivana Ivanovic-Burmazovic,[§] Dean D. Schwartz,[¥] and Christian R. Goldsmith[†,*]

[†]Department of Chemistry and Biochemistry, Auburn University, Auburn, AL 36849, United States (USA)
[§]Department of Chemistry and Pharmacy, University Erlangen-Nuremberg, 91058 Erlangen, Germany
[‡]Auburn University Magnetic Resonance Imaging Research Center, Auburn, AL 36849, USA
[¶]Department of Pathobiology, College of Veterinary Medicine, Auburn University, Auburn, AL 36849, USA
[¥]Department of Anatomy, Physiology, and Pharmacology, College of Veterinary Medicine, Auburn University, Auburn, AL 36849, USA

*To whom correspondence should be addressed: crgoldsmith@auburn.edu

Table of Contents

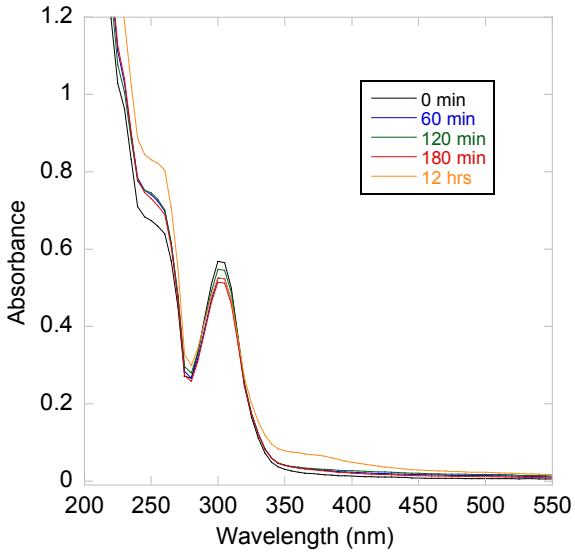

Figure S1. UV/Vis spectra depicting the stability of a 0.10 mM solution of [Mn(H_4qtp2)Br_2] (**2**) in MeOH to air. The reaction was scanned at 0, 1, 2, 3, and 12 h. The band at 302 nm is characteristic of quinol functional groups.

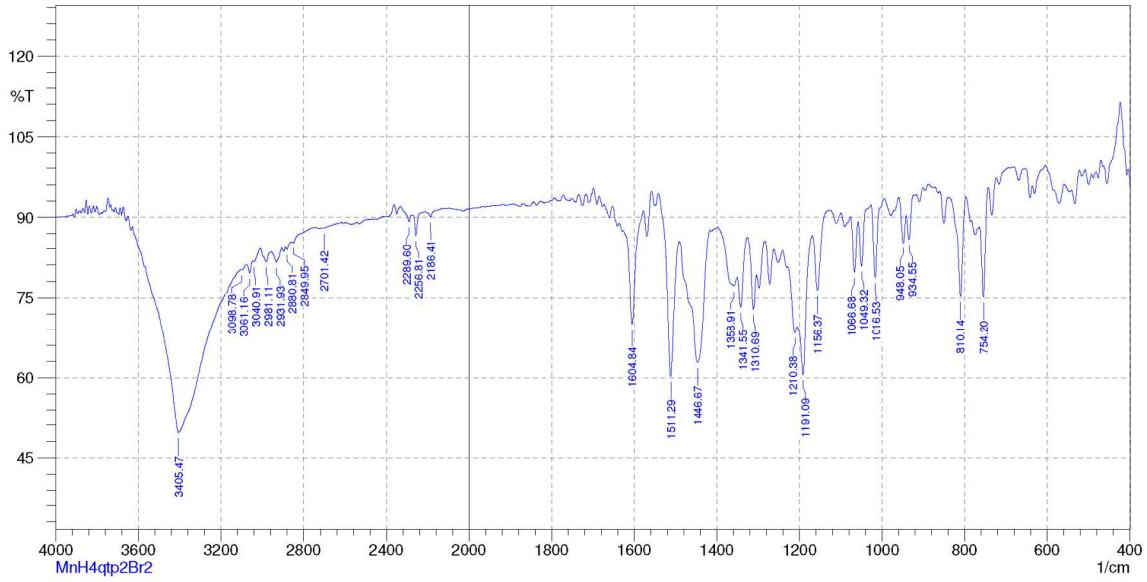

Figure S2. IR spectrum of **2** (KBr). The 3405 cm^{-1} feature is assigned to the O-H stretches associated with the quinol groups of the H_4qtp2 ligand. The 1605 cm^{-1} feature is assigned to the C-N stretches associated with the metal-coordinated pyridine rings.

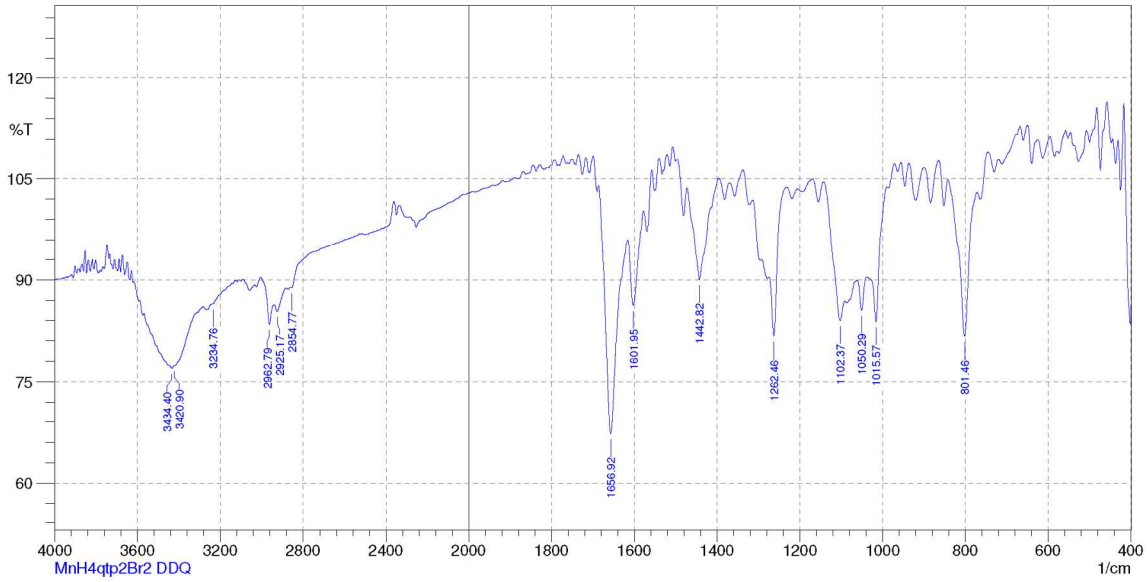

Figure S3. IR spectrum of **3 (**KBr). This compound was prepared cleanly from the oxidation of **2** by 2,3-dichloro-5,6-dicyano-1,4-benzoquinone (DDQ). The peak at 1657 cm^{-1} is assigned to the C=O stretches of the quinone subunits.

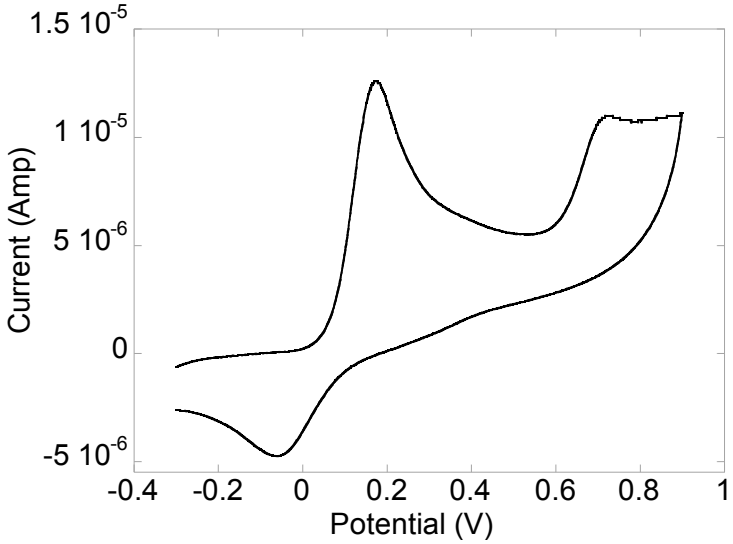

Figure S4. Cyclic voltammetry of 1.0 mM **2** in 0.10 M phosphate buffer (NaH_2PO_4/Na_2HPO_4, pH=7.2). The scan rate was 100 mV/s. For the quasi-reversible feature: $E_{1/2}$ = 57 mV vs. Ag/AgCl, ΔE = 232 mV. An irreversible feature with *E*pc = 725 mV is also observed.

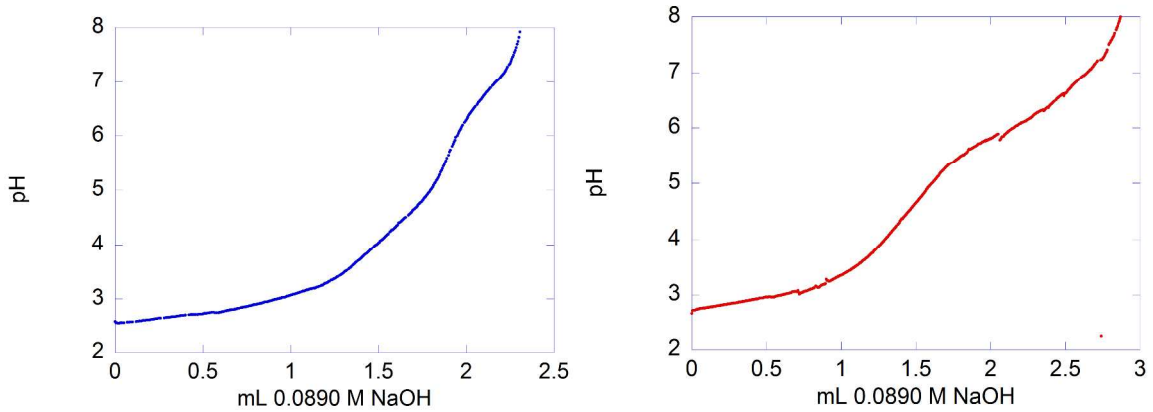

Figure S5. Raw potentiometric pH titration data for the addition of 0.08903 M KOH to acidic aqueous solutions containing 100 mM KCl and either A) 1.0 mM H_4qtp2 or B) 0.82 mM **2**. Each titration was performed at 25 °C under an argon atmosphere. For the titration displayed in B), precipitation was observed at about pH 8.0. A titration with 1.0 mM H_4qtp2 and 1.0 mM $MnCl_2$ provided ionization events identical within error to that in panel B.

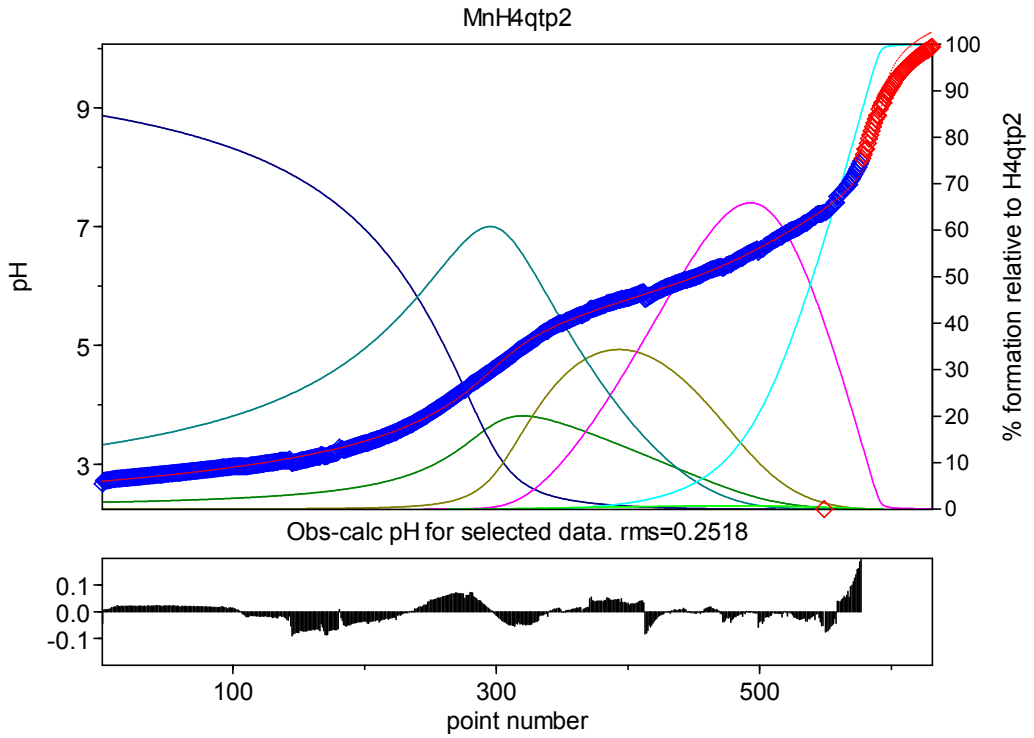

Figure S6. Hyperquad model (red line) overlaid on the experimental data from **Figure S5** (blue). The data above pH 8 have been excluded from the calculations since precipitation was observed above this value. The parameters for the Hyperquad model are provided on Table 3. The fit assumes an initial total of 0.178 mmol H^+. The residuals for the fit are provided below. The curves represent the formation of various species including [Mn(H_2qtp2)] (light blue), $[Mn(H_3qtp2)]^+$ (purple), $[Mn(H_4qtp2)]^{2+}$ (olive green), $[Mn(H_5qtp2)]^{3+}$ (pine green), H_5qtp2^+ (aqua), and H_6qtp2^{2+} (dark blue).

Table S1. Parameters for the Hyperquad model used in **Figure S6**.

Species	Mn^{2+}	H_4qtp2	H^+	log(β)	Derived Values
H_4qtp2	0	1	0	0.00	
$\mathbf{H_5}qtp2^+$	0	1	1	7.18 (±0.03)	pK_{L2} = 7.18 (±0.03)[a]
$\mathbf{H_6}qtp2^{2+}$	0	1	2	11.65 (±0.05)	pK_{L1} = 4.47 (±0.08)[a]
$[Mn(H_2qtp2)]$	1	1	-2	-7.19 (±0.01)	
$[Mn(\mathbf{H_3}qtp2)]^+$	1	1	-1	-0.05 (±0.01)	$pK_a(Mn(H_3qtp2)^+)$ = 7.14 (±0.02)[b]
$[Mn(\mathbf{H_4}qtp2)]^{2+}$	1	1	0	5.77 (±0.01)	$pK_a(Mn(H_4qtp2)^{2+})$ = 5.82 (±0.02)[c]
$[Mn(\mathbf{H_5}qtp2)]^{3+}$	1	1	1	11.30 (±0.01)	$pK_a(Mn(H_5qtp2)^{3+})$ = 5.53 (±0.02)[d]

Refer to Scheme 4 for the proposed molecular structures for each ligand and Mn(II) complex. Due to the instability of the ligand at high pH values, we were unable to obtain log(β) values for the H_3qtp2^- and H_2qtp2^{2-} species.

[a]Ligand pK_a values corresponding to the (de)protonation of the free ligand amine and pyridine groups. $K_{L1} = [H_5qtp2^+][H^+]/[H_6qtp2^{2+}]$, $pK_{L1} = \log\beta_{011} - \log\beta_{010}$. $K_{L2} = [H_4qtp2][H^+]/[H_5qtp2^+]$, $pK_{L2} = \log\beta_{012} - \log\beta_{011}$.

[b]$K_a(Mn(H_3qtp2)^+) = [Mn(H_2qtp2)][H^+]/[Mn(H_3qtp2)^+]$, corresponds to the (de)protonation of the second quinol. $pK_a(Mn(H_3qtp2)^+) = \log\beta_{11\text{-}1} - \log\beta_{11\text{-}2}$.

[c]$K_a(Mn(H_4qtp2)^{2+}) = [Mn(H_3qtp2)^+][H^+]/[Mn(H_4qtp2)^{2+}]$, corresponds to the (de)protonation of a quinol group. $pK_a(Mn(H_4qtp2)^{2+}) = \log\beta_{110} - \log\beta_{11\text{-}1}$.

[d]$K_a(Mn(H_5qtp2)^{3+}) = [Mn(H_4qtp2)^{2+}][H^+]/[Mn(H_5qtp2)^{3+}]$, corresponds to the (de)protonation of a pyridine group. $pK_a(Mn(H_5qtp2)^{3+}) = \log\beta_{111} - \log\beta_{110}$.

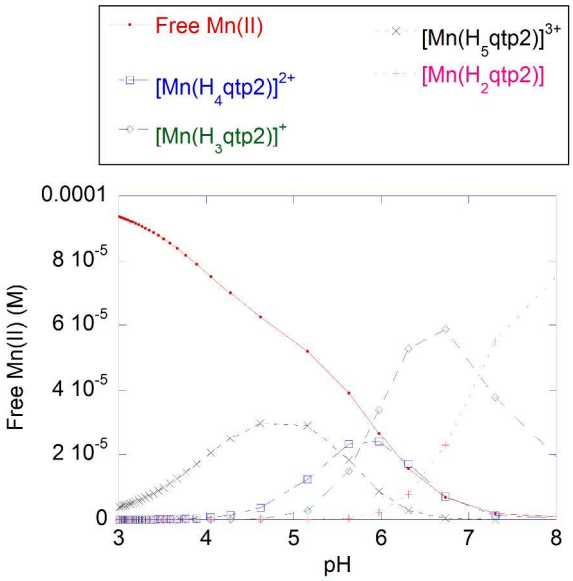

Figure S7. Predicted speciation as a function of pH for **2** at 100 μM.

High Pressure Liquid Chromatography (HPLC)

HPLC was performed using an Agilent 1200 series apparatus with UV detection at 254 nm and a Waters μBondapak C18 Column (3.9 × 300 mm). The following eluents were used: A) 95% MeCN/5% 10 mM ammonium acetate, B) 10 mM ammonium acetate, C) H_2O/0.1% formic acid, D) MeCN/0.1% formic acid. The following methods were used:

(1) gradient 5% A and 95% B to 95% A and 5% B over 14 min with a 4 min wash of 5% A and 95% B in between samples. Flow rate = 0.8 mL/min. Injection volume = 10 μL.

(2) gradient 5% C and 95% D to 95% C and 5% D over 14 min with a 4 min wash of 5% C and 95% D in between samples. Flow rate = 0.8 mL/min. Injection volume = 10 μL.

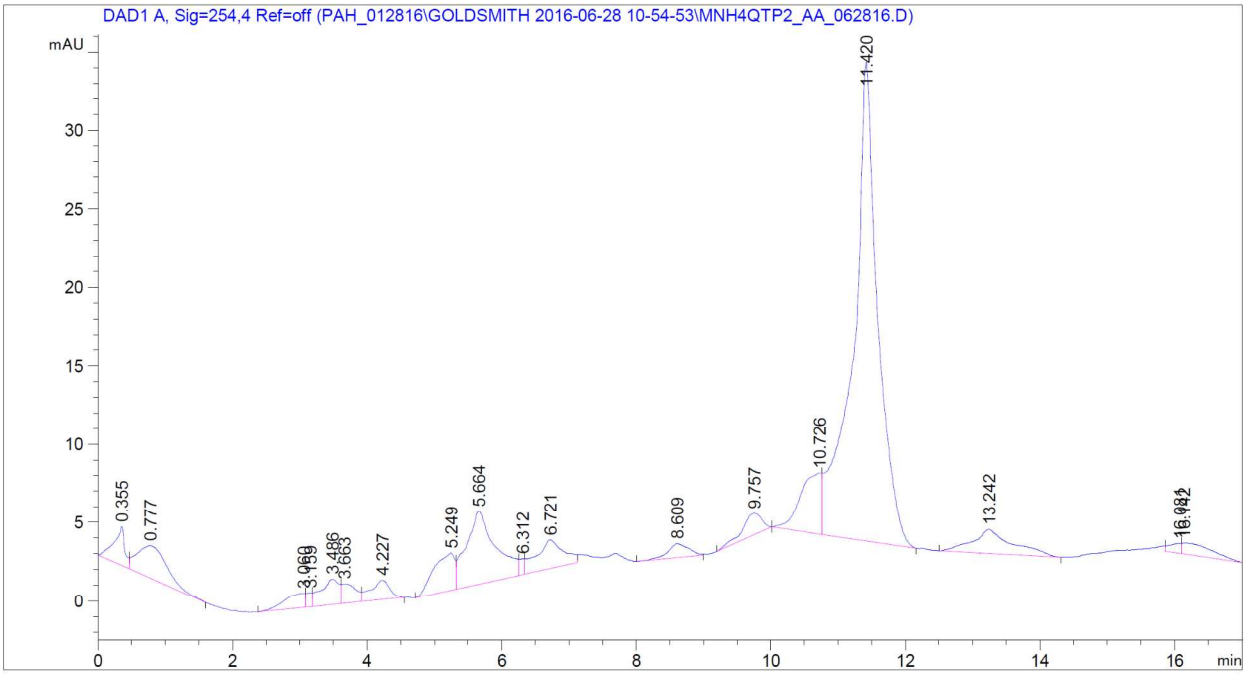

Figure S8. LC trace for **2** run under method 1. The pH of the ammonium acetate buffer was found to be 7.35. The free H_4qtp2 ligand appears at 6.70 min when run under identical conditions. The other peaks aside from the major one at 11.420 min are irreproducible.

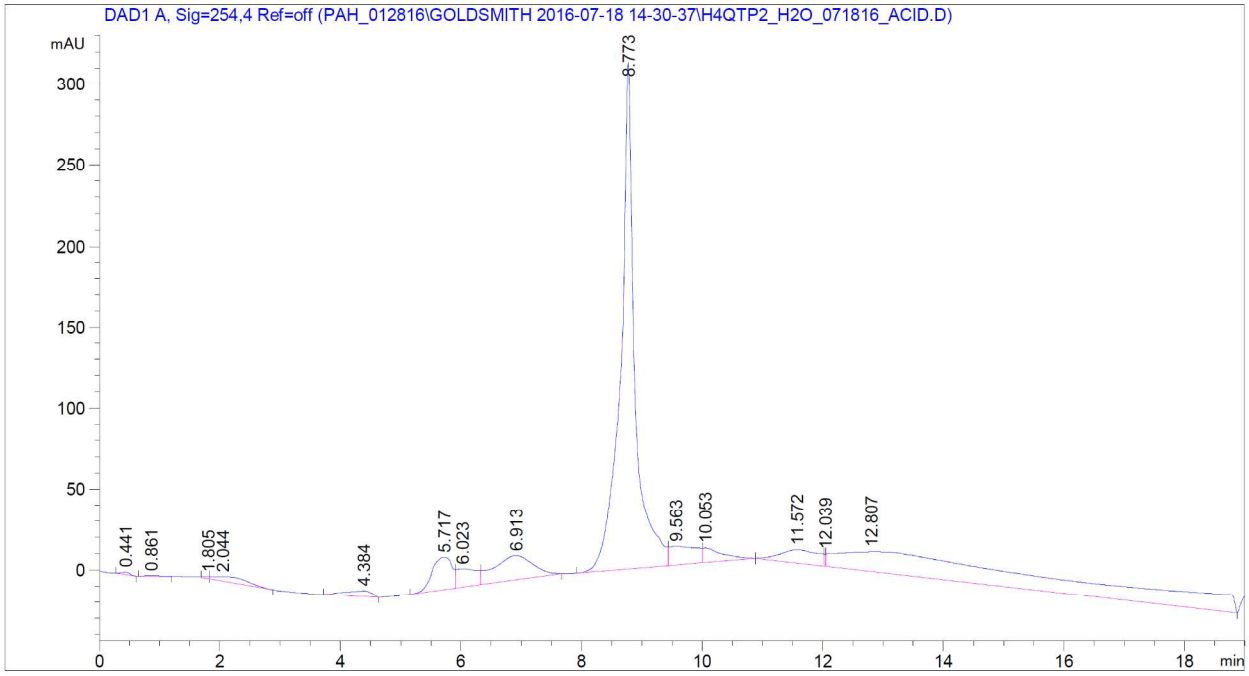

Figure S9. LC trace for H_4qtp2 run under method 2. The other peaks aside from the major one at 8.773 min are irreproducible.

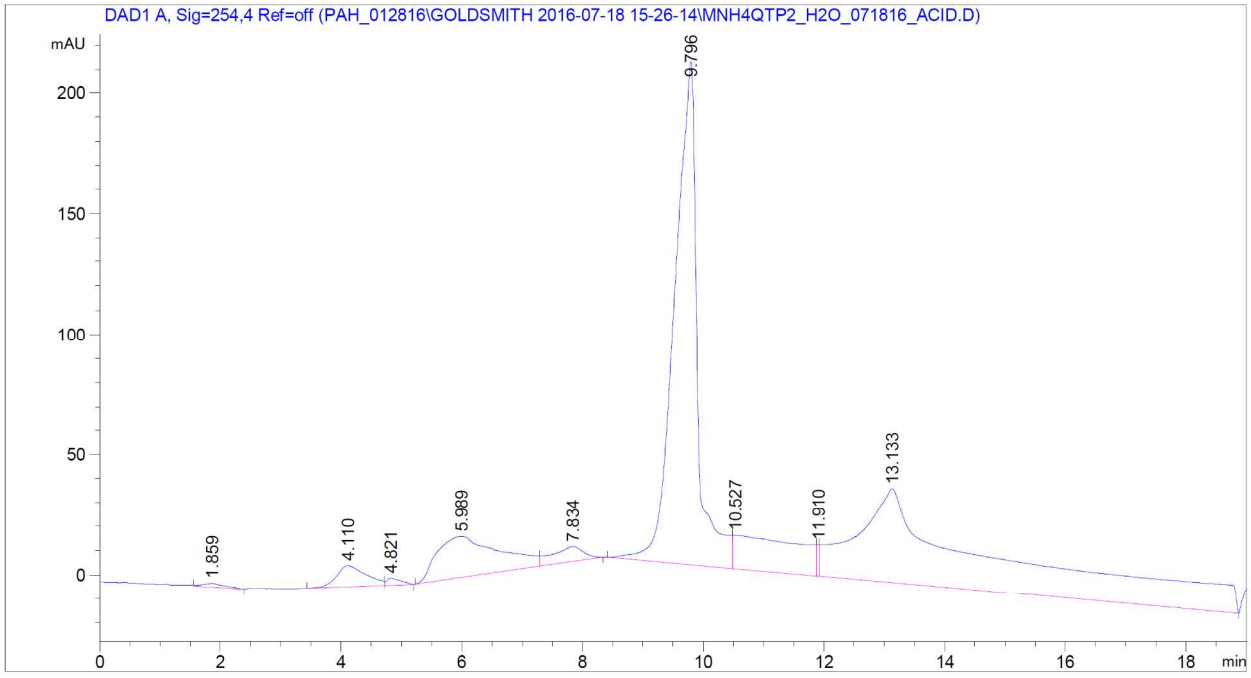

Figure S10. LC trace for **2** run under method 2.

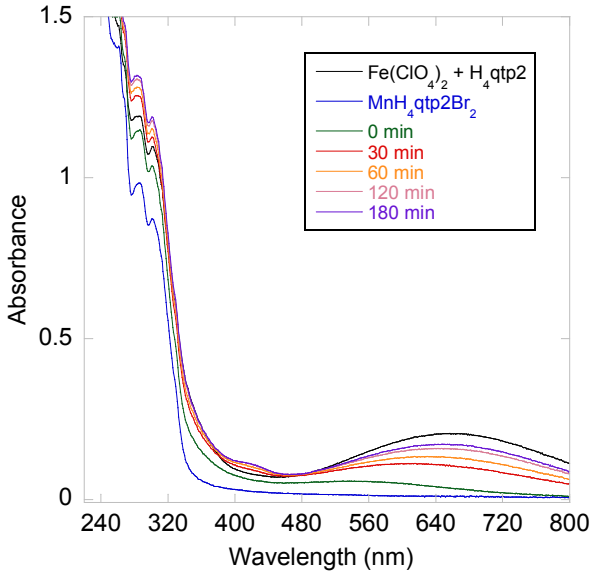

Figure S11. Spectrophotometric analysis of the reaction between 0.10 mM $Fe(ClO_4)_2$ and 0.10 mM **2** in MeOH at 298 K. The UV/vis spectrum of the product formed from 0.10 mM $Fe(ClO_4)_2$ and 0.10 H_4qtp2 (black) and that corresponding to 0.10 mM **2** are provided for comparison. Approximately 80% of Mn(II) has been replaced by Fe(II) by 3 h.

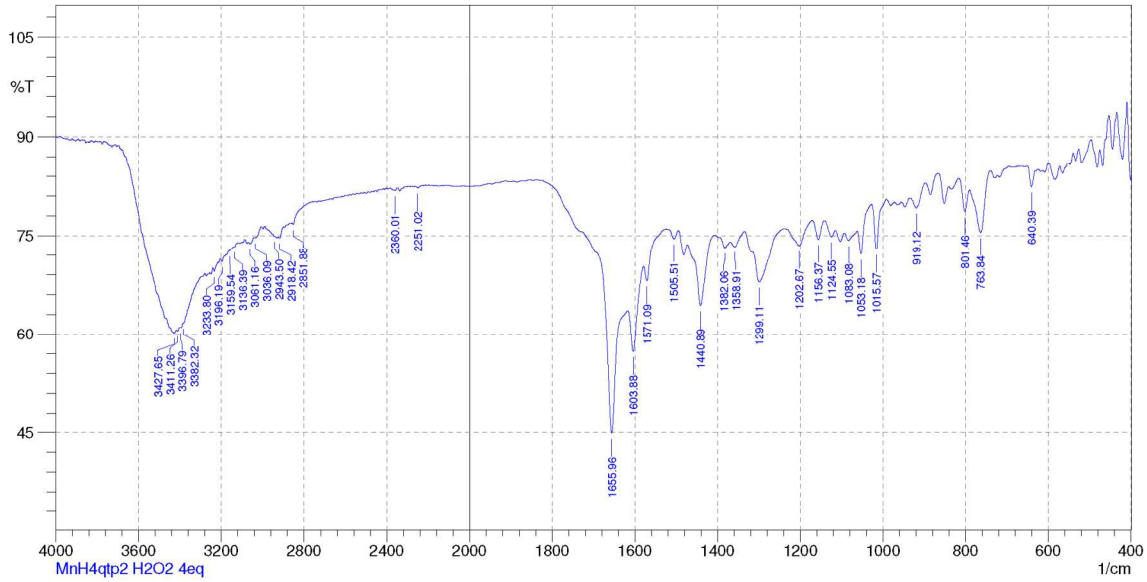

Figure S12. IR spectrum of the crude product from the reaction between 1.0 mM **2** and 4.0 mM H_2O_2 in MeOH. After allowing 30 min to react, the solvents were stripped, yielding the solid used to prepare the sample (KBr). The peak at 1659 cm^{-1} is assigned to a C=O stretch for the quinone groups formed upon the partial oxidation of the H_4qtp2 ligand.

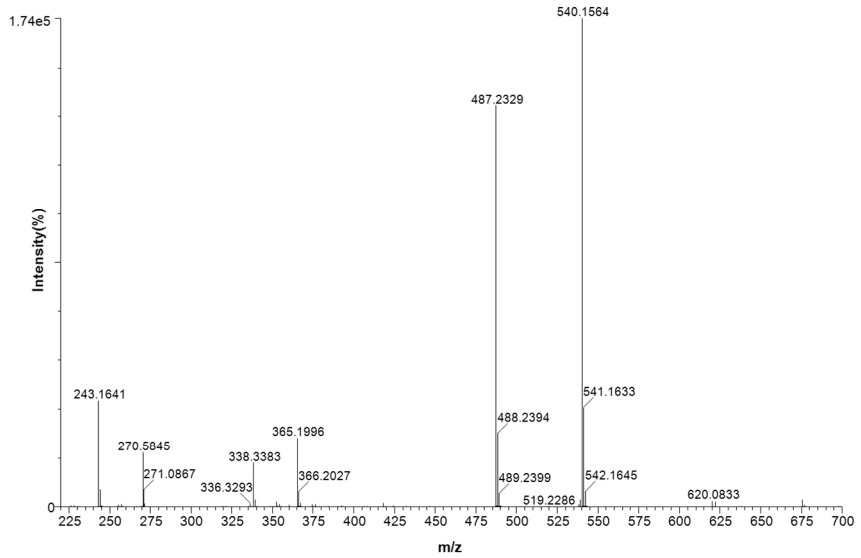

Figure S13. Mass spectrometry (ESI) of **2** in MeOH. The 540.1564 m/z feature is assigned to the singly deprotonated Mn(II) complex $[Mn(H_3qtp2)]^+$ (calculated m/z = 540.1569). The 487.2329 m/z feature is assigned to $[H_5qtp1]^+$, the singly protonated ligand (calculated m/z = 487.2345).

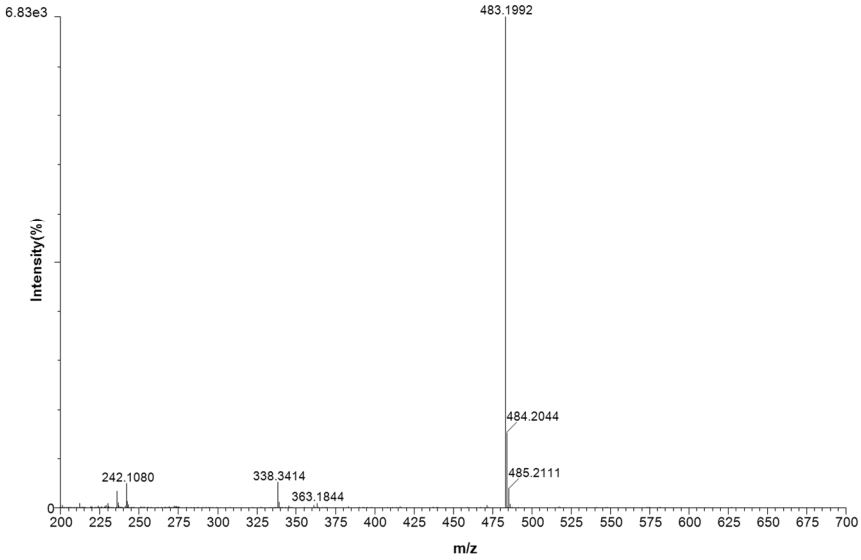

Figure S14. Mass spectrometry (ESI) of $[Mn(qtp2)Br_2]$ (**3**) in MeCN. The 483.1992 m/z feature is assigned to $[Hqtp2]^+$, the singly protonated form of the diquinone qtp2 ligand (calculated m/z = 483.2032).

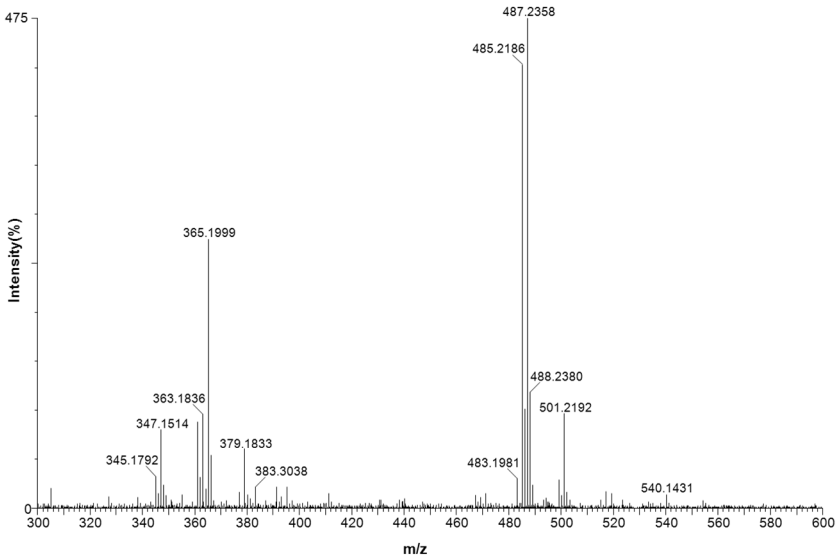

Figure S15. Mass spectrometry (ESI) of a mixture of **2** in H_2O and 4 equiv. of H_2O_2. The reaction was allowed to proceed for 30 min. The 483.1981 m/z feature is assigned to [**Hqtp2**]$^+$ (calculated m/z = 483.2032), the singly protonated form of the fully oxidized (diquinone) ligand. The 485.2186 m/z feature is assigned to [**H$_3$qtp2**]$^+$ (calculated m/z = 485.2189), the singly protonated form of the partially oxidized (monoquinone) ligand, H_2qtp2. The 487.2358 m/z feature is assigned to [H_5qtp1]$^+$ (calculated m/z = 487.2345).

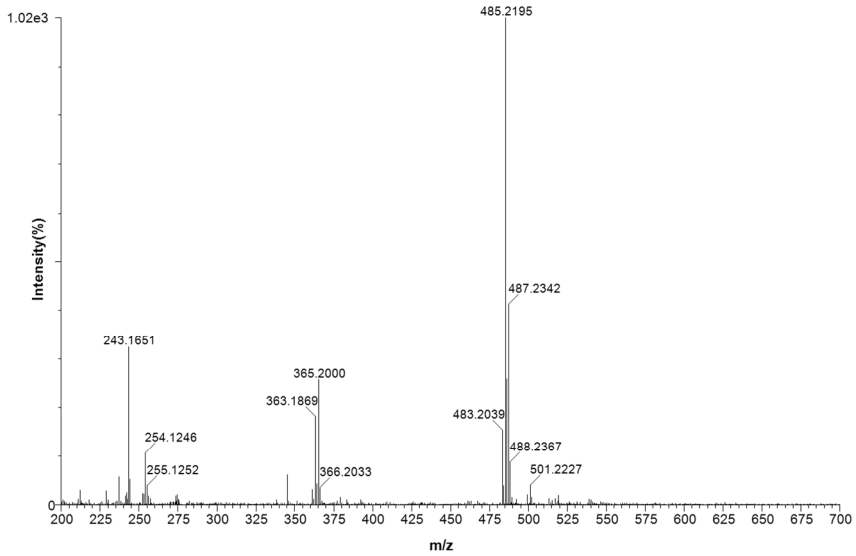

Figure S16. Mass spectrometry (ESI) of a reaction between **2** and 4 equiv. of H_2O_2 in MeOH. The reaction was allowed to proceed for 60 min. The 483.2039 m/z feature is assigned to [**Hqtp2**]$^+$ (calculated m/z = 483.2032), the singly protonated form of the fully oxidized (diquinone) ligand. The 485.2195 m/z feature is assigned to [**H$_3$qtp2**]$^+$ (calculated m/z = 485.2189), the singly protonated form of the partially oxidized (monoquinone). The 487.2342 m/z feature is assigned to [H_5qtp1]$^+$ (calculated m/z = 487.2345), the singly protonated form of the non-oxidized ligand.

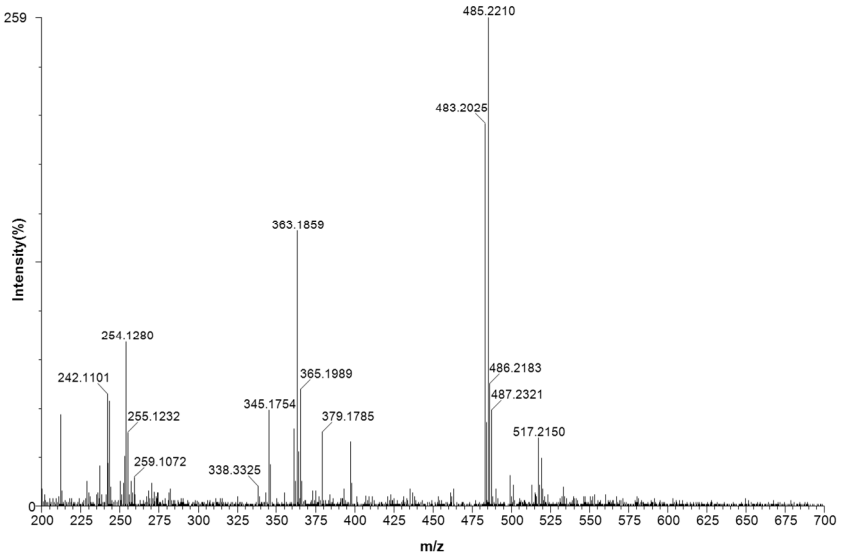

Figure S17. Mass spectrometry (ESI) of a reaction between **2** and 8 equiv. of H_2O_2 in MeOH. The reaction was allowed to proceed for 60 min. The 483.2025 m/z feature is assigned to [**Hqtp2**]$^+$ (calculated m/z = 483.2032). The 485.2210 m/z feature is assigned to [**H_3qtp2**]$^+$ (calculated m/z = 485.2189). The 487.2321 m/z feature is assigned to [H_5qtp1]$^+$ (calculated m/z = 487.2345).

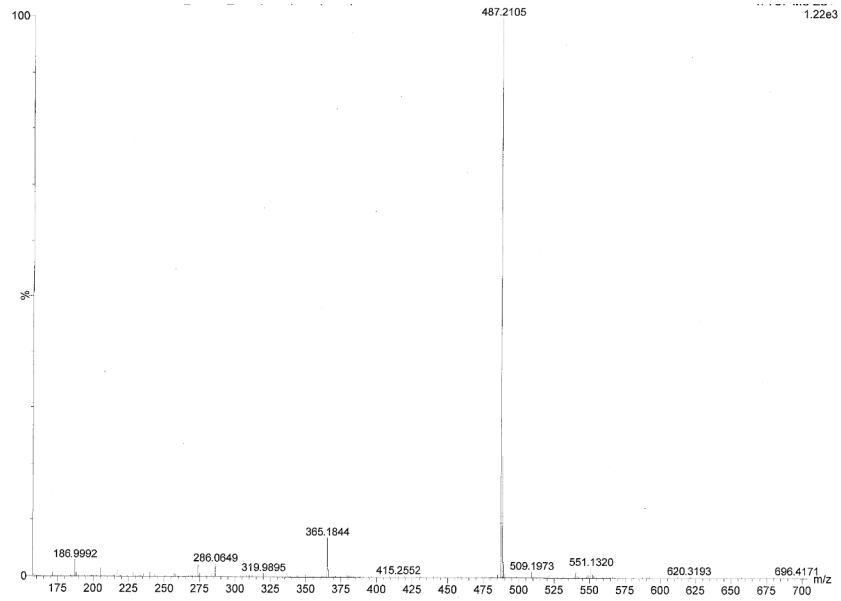

Figure S18. Mass spectrometry (ESI) a sample of **2** that was sequentially oxidized by H_2O_2 and reduced by sodium dithionite ($Na_2S_2O_4$). Complex **2** first reacted with 4 equiv. of H_2O_2 for 60 min at RT in MeOH. The solvent and excess H_2O_2 was removed and the crude was allowed to react with 4 equiv. of Na_2SO_4 for an additional 60 min. The excess Na_2SO_4 was removed via filtration prior to analysis. The 487.2105 m/z feature is assigned to [H_5qtp1]$^+$ (calculated m/z = 487.2345).

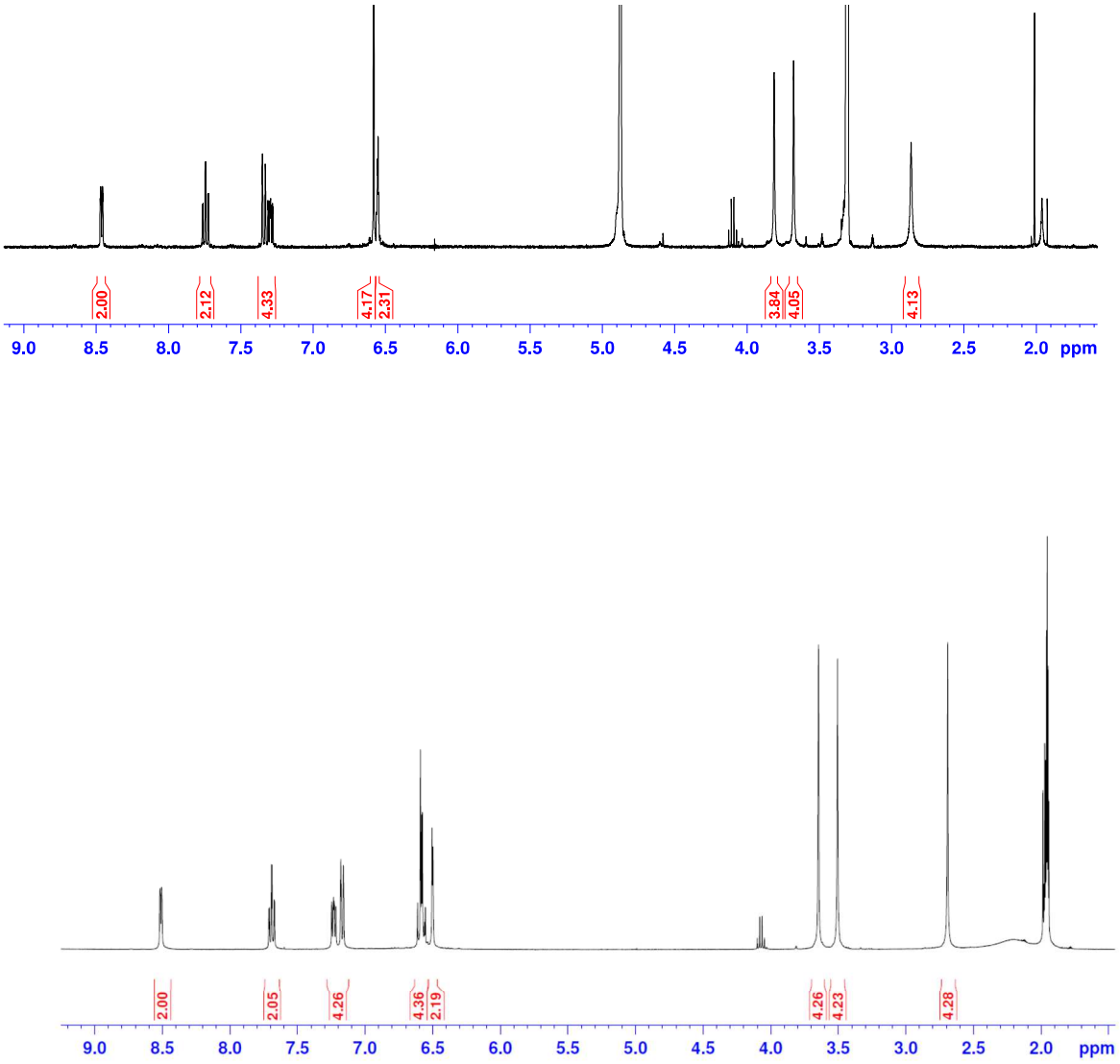

Figure S19. ^{1}H NMR spectra of H_4qtp2 in CD_3OD (top) and CD_3CN (bottom). The peaks at ~6.5 ppm can be attributed to the O-H and C-H protons on the quinol subunits.

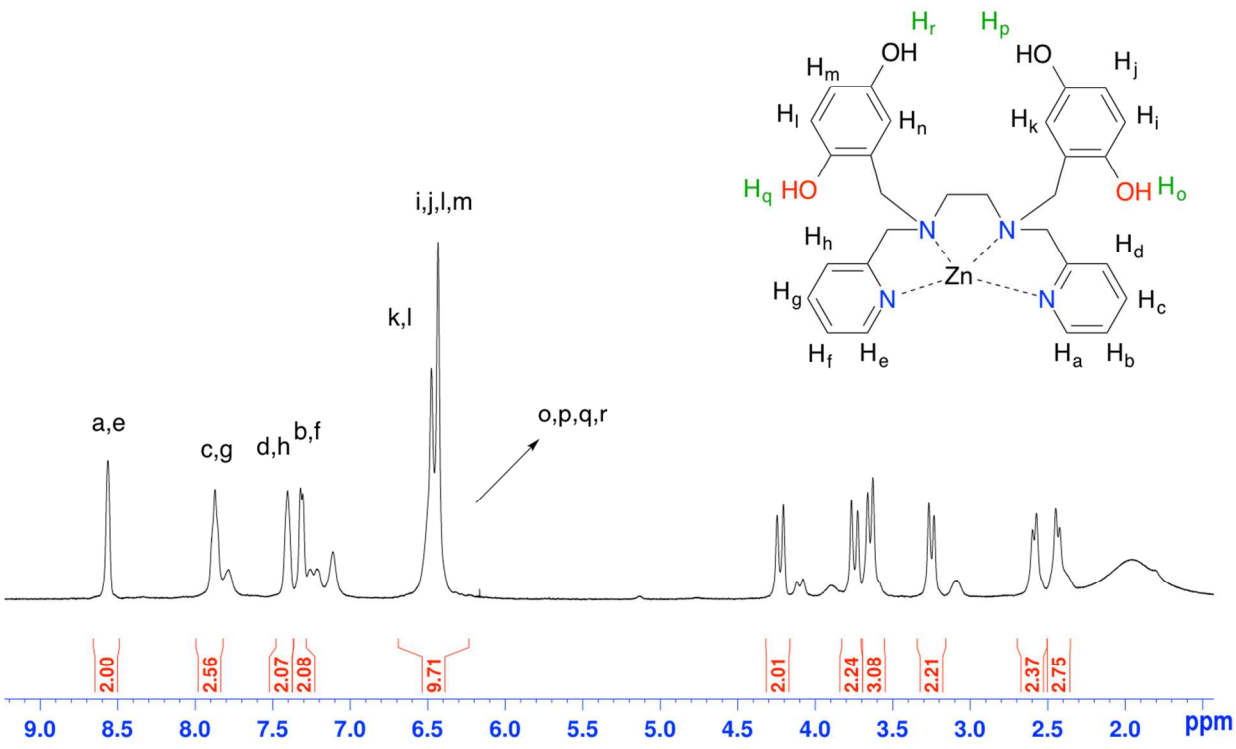

Figure S20. ^{1}H NMR spectrum of the diamagnetic product from the reaction between 10 mM **2** and 20 mM $Zn(ClO_4)_2$ in CD_3CN. The reaction was given 2 h to equilibrate. The peaks observed between 7.0 and 8.8 ppm can be assigned to the protons on the pyridine subunits. The peaks around 6.5 ppm can be attributed to the O-H and C-H protons on the quinol subunits.

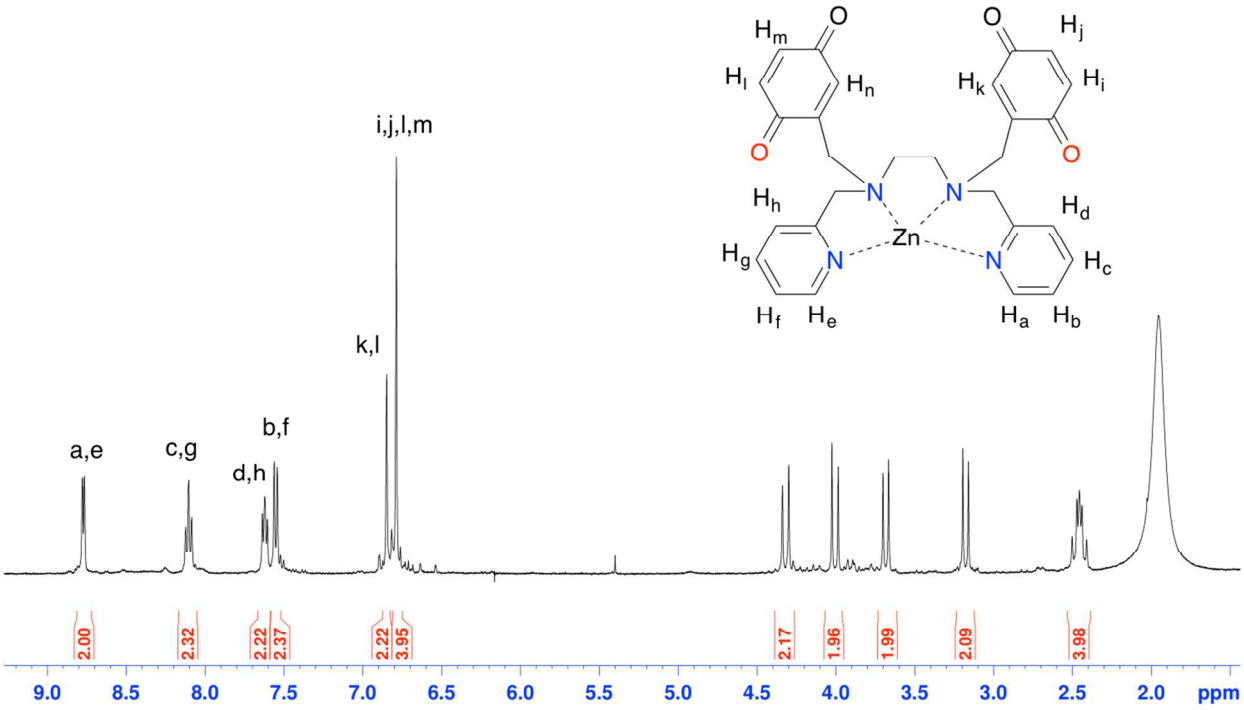

Figure S21. ^{1}H NMR spectrum of the diamagnetic product from the reaction between 10 mM **3** and 20 mM $Zn(ClO_4)_2$ in CD_3CN. The reaction was given 2 h to equilibrate. The decreased intensities of the peaks at ~6.8, relative to those in **Figure S20**, correspond to a loss of 4 H nuclei upon oxidation.

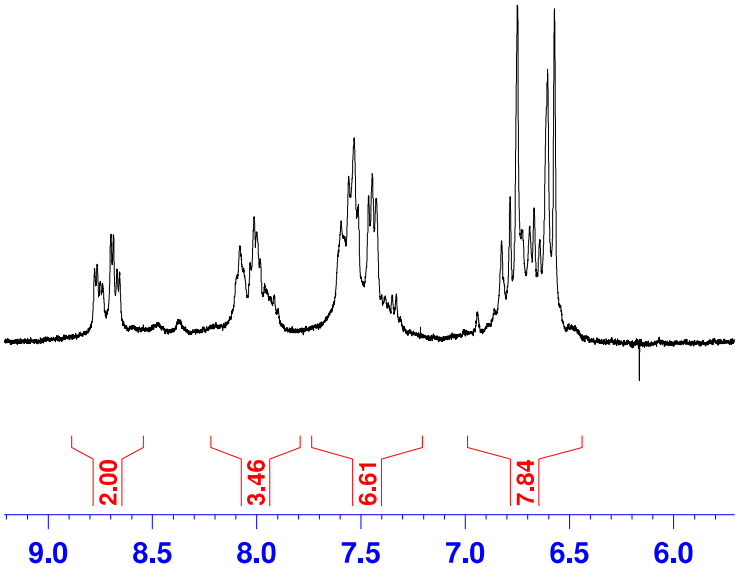

Figure S22. ^{1}H NMR spectrum of the diamagnetic product between **2**, 4 equiv. of H_2O_2, and 2 equiv. of $Zn(ClO_4)_2$ in CD_3CN. The Mn(II) complex and H_2O_2 were allowed to react for 1 h. The subsequent reaction with Zn(II) was provided 2 h to equilibrate. The spectrum is consistent with a mixture of the species observed in **Figures S20** and **S21**. Approximately 55% of the quinols have been oxidized.

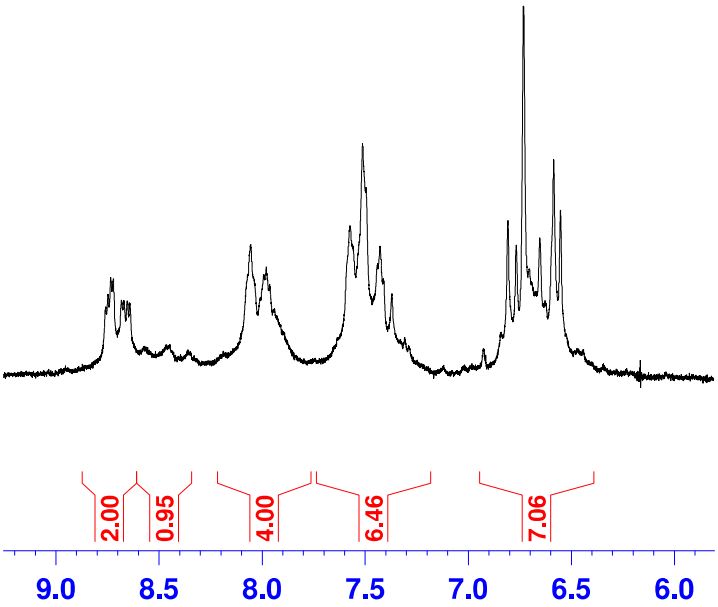

Figure S23. ^{1}H NMR spectrum of the diamagnetic product between **2**, 8 equiv. of H_2O_2, and 2 equiv. of $Zn(ClO_4)_2$ in CD_3CN. The Mn(II) complex and H_2O_2 were allowed to react for 1 h. The subsequent reaction with Zn(II) was provided 2 h to equilibrate. The spectrum is consistent with a mixture of the species observed in **Figures S20** and **S21**. Approximately 75% of the quinols have been oxidized to *para*-quinones.

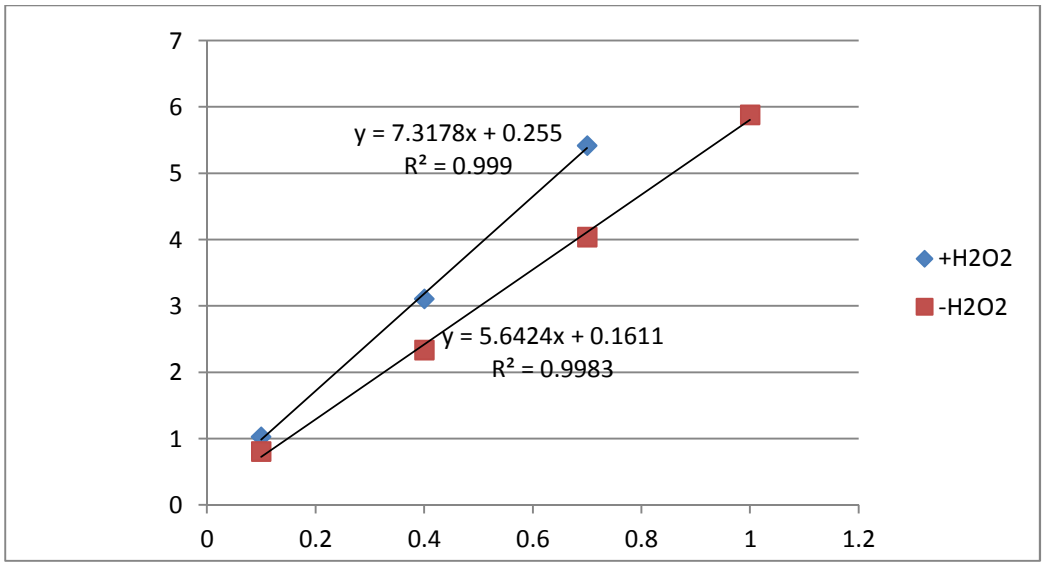

Figure S24. Plots of ($1/T_1$) versus Mn(II) concentration for **2** in the presence (blue) and absence (red) of 10 mM H_2O_2. All samples were run in 298 K aqueous solutions containing 50 mM HEPES buffered to pH 7.00, using a 3 T field provided by a clinical MRI scanner. The data were fit to the indicated linear equations; the y-intercepts were within error of $1/T_1$ measurements associated with two control samples that contained no Mn(II): pure water (0.39 s^{-1}) and 50 mM HEPES buffer (0.38 s^{-1}). These data replicate the results shown in **Figure 8**.

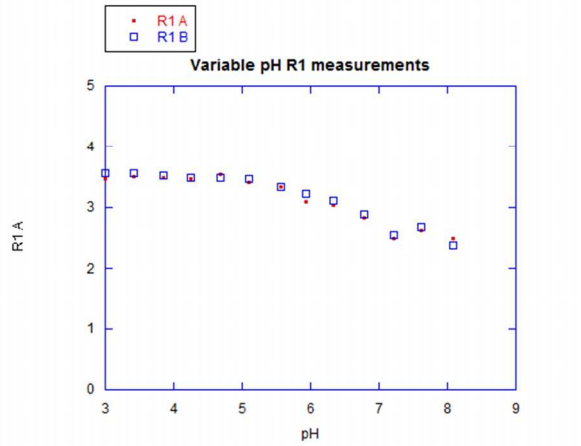

Figure S25. Plots of R_1 ($1/T_1$) versus pH for a 0.50 mM solution of **2** in unbuffered water. The pH was controlled via the addition of HCl and KOH. All samples were analyzed at 298 K using a 3 T field provided by a clinical MRI scanner.

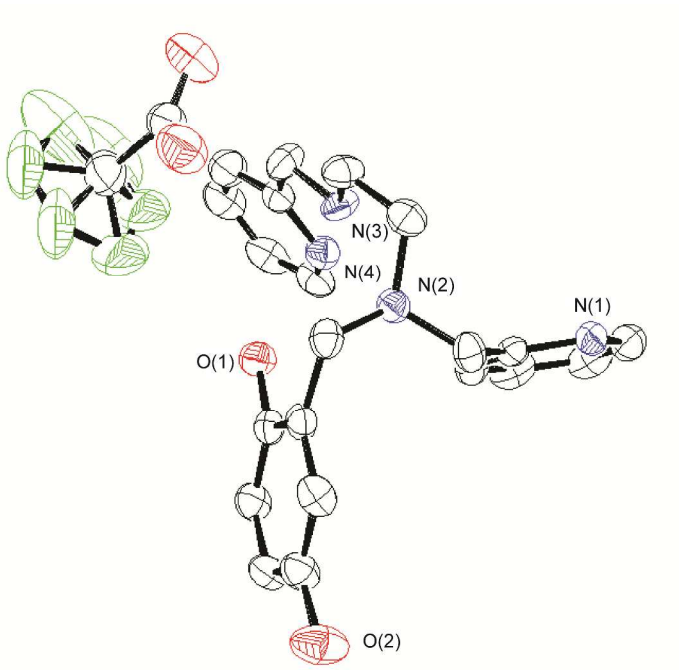

Figure S26. ORTEP representation of the ligand precursor *N*-(2,5-Dihydroxybenzyl)-*N,N'*-bis(2-pyridinylmethyl)-1,2-ethanediammonium trifluoroacetate. All thermal ellipsoids are drawn at 50% probability. Hydrogen atoms are excluded for clarity. The CF_3 group on the trifluoroacetate ion is disordered over two positions. The crystals were grown by diffusing ether into a MeOH solution of crude *N*-(2,5-Dihydroxybenzyl)-*N,N'*-bis(2-pyridinylmethyl)-1,2-ethanediamine.